Synthesis, morphology, crystal structure, optical and dielectric properties of Ba_2NiWO_6 new tungsten double perovskite.

Yousef A. Alsabah[1, 2, 4], Abdelrahman A. Elbadawi[1], Mohamad S. AlSalhi[2, 3], Eltayeb M. Mustafa[1].

1. Department of Physics, Faculty of Science and Technology, Al Neelain University, Khartoum, Sudan.
2. Research Chair in Laser Diagnosis of Cancers, College of Science, King Saud University, Riyadh, Kingdom of Saudi Arabia.
3. Department of Physics and Astronomy, College of Science, King Saud University, Riyadh, Kingdom of Saudi Arabia.
4. Department of Physics, Faculty of Education and Applied Science, Hajjah University, Hajjah, Yemen.

Abstract:

Using solid state reactoin method, Tungsten double perovskite oxides Ba_2NiWO_6 have been prepaired. The X ray diffration XRD, Scanning electronic microscopy SEM, Ultravielot.visible diffuse reflection, Photoluminescence spectra and Electrical impedance spectroscopy were used to charactrize the structure and optical properites of the synthesized material. From X ray powder diffration examination, the sample shows a cubic structure with (Fm-3m) space group, and the lattice parameter was investgated using Retvield method that found to be 8.10875 Angestrom. The band gap energy of Ba_2NiWO_6 estimated to be 3.20 eV from the diffuse reflection spectrum. At room temperature the excitation and emission photolumenescence and EIS have been investgated.

Keywords: double perovskite, XRD, SEM, UV-visible diffuse reflectance, Raman, EIS, luminescence PL.

1. Introduction

Gustav Rose in 1839 was discovered the mineral perovskite from samples obtained in the Ural Mountains. The term perovskite was originally reserved for the mineral $CaTiO_3$. The first synthetic perovskites were produced in1929 by Goldschmid of the University of Oslo led to the use of the term perovskite as a description of a class of compounds sharing the same general stoichiometry and connectivity found in $CaTiO_3$ [1-3].

Natural perovskites make up much of the Earth's mantle (50-90%) in the form of $MgSiO_3$. The dense packing of the perovskite structure makes it ideal for high pressure environments like this. It is believed to be the most abundant mineral within the Earth. The perovskite structure is also a part of many materials whose properties make them useful in industry, from ferroelectric behavior to superconductivity and colossal magnetoresistance[3].

Double peroviskite material took the attention of many researchers due to their interesting structural, magnetic and electrical properties. The general chemical formula of double perovskite oxides expressed in $A_2BB`O_6$, where A is Ca,Sr , Ba ( one of the elements of the first group or the second group in the periodic table) and B site is ocuppied by first row of 3d magnetic element in the perodic table. The B` site is ocuppied by the 4d non-magnetic elements, with O atom located in between forming alternate BO_6 octahedral and B-O-B bonds, The wide range of double perovskite material is due to alteration at the magnetic and non –magnetic of B and B` elements as well as the A-site cations[4-10].

In particular, the compositions Ba_2BMoO_6, where B = Fe, Mn, Cr are magnetic ions are currently studied for their potentiality as magnetoresistive systems and thermoelectrics[11].

The synthesis and structural properties of new Dy_2MgTiO_6 and Gd_2MgTiO_6 perovskite -like material was performed. thier materials crystallize in monoclinic double perovskites with space group $P2_1/n$ that showed by Rietveld analyses. Dy_2MgTiO_6 and Gd_2MgTiO_6 perovskite had a paramagnetic behavior, which was refined by the Curie–Weiss model. The experimental cell magnetic moment supplies the values 14.4 μ_B and 10.8 μ_B for Dy_2MgTiO_6 and Gd_2MgTiO_6, respectively. These double perovskite compounds had semiconducting behavior, which showed by Density of states results, with energy gap between 0.6 eV and 0.73 eV and effective magnetic moment of 13.9 μ_B and 10.1 μ_B for Dy_2MgTiO_6 and Gd_2MgTiO_6, consecutively, which are majority due to the f-orbitals of the rare earth cations[12].

$ALaFeTiO_6$ (A= Ba,Sr andCa) double perovskite oxides of chemical mode had been done by following the precursor method, and the structural analysis of $BaLaFeTiO_6$ is cubic and in consistency with it's tolerance factor. The alteration of crystal structure from higher symmetry to lower symmetry showed, as the size of the A-site decreases due to the substitution in the A-site . The Weak ferromagnetism had been showed under both the internal pressure and the anti-site effect which facilitate the appearance of the $\uparrow Fe^{3+}$-O-$Fe^{3+}\downarrow$ antiferromagnetic interaction with canted spin[9].

La_{1-x} K_xMnO_3 perovskites (x = 0.1, 0.125 and 0.150) had prepared by solid-state reaction method, rhombohedrally-distorted structure showed by The Rietveld refinements of X-ray diffraction patterns. on application of 5 T field and at about 244, 259, and 280 K, respectively The resistivity of all the samples exhibit metaleinsulator transition,. At low temperatures (<30 K), resistivity showed an upturn

which on application of magnetic field ~ 5 T suppresses. The small polaron conduction is adequate to explain semiconducting resistivity (H = 0, 5 T)[13].

spin-reorientation situation of $YFe_{1-x}Mn_xO_3$ (x = 0.0, 0.2) perovskite showed and corroborated by magnetic properties and Massbauer spectroscopy. the spin-reorientation transition temperature (TSR) increment when the Neel temperature (TN) decrement with increasing x, under the weakening of the exchange interaction between Fe ions. They shown occurrence of spin- reorientation relative to crystal axes from the Muossbauer spectra of $YFe_{1-x}Mn_xO_3$ (x = 0.1, 0.2). and the Neel temperature TN for $YFe_{0.85}Mn_{0.15}O_3$ was calculated to be 580K (10). The canting angle between the Fe sublattices in $YFe_{0.85}Mn_{0.15}O_3$ at 200 K is calculated to be 1.58 mrad[14].

In this study, we will use the X-ray diffraction, scanning electronic microscopy, FTIR spectroscopy, Raman spectroscopy, photo luminesces spectroscopy, UV-Vis diffuse reflectance and Impedance spectroscopy to study the structure, optical and dielectric properties of the Ba_2NiWO_6 double perovskite behavior.

2. Experimental

2.1. Materials and Solid-state reaction Preparation

All first material purchased from Alfa Acer were obtained; $BaCO_3$, WO_3, and NiO with 99.99% purity. Using solid-state reaction method, the Ba_2NiWO_6 double perovskite was prepared. The sample were prepared by mixing $BaCO_3$ (barium carbonite), WO_3 (tungsten trioxide) and (nickel oxide) NiO, many of different treatments in order to get single phase for the samples. The mixtures of compounds grinded in agate mortar with the addition of acetone and then kept in crucibles and heated in air at 800 ^oC for 12 hours two times; the sample pellet in around shape and heated in/at 1000 °C two times and the sample pellet in around shape and heated in/at 1200 °C two times, respectively. It permeates every step heating treatment the sample grinding for two hours with the process of add the amount of acetone to increase the homogeneity of the sample with the rate of 10 ^oC per minute during the heating process and cooling as well. The ratio of the amounts calculated by the following equation:

$$2BaCo_3 + NiO + WO_3 \rightarrow Ba_2NiWO_6 + 2CO_2 \uparrow \qquad (1)$$

2.2. X- ray powder diffraction

X-ray diffraction (XRD) data collected by a Bruker - axs D8 using CuKα radiation (λ=1.54Å). At room temperature, with a nickel filter operating at 40 KV, 40 mA the data collected for the 2θ in 0.02-step size and five-second count time in 20^o - 80^o range. The fullprof suite program [15] used for the XRD date analysis by Rietveld refinement method. The crystalline size (D) calculated by Scherer equation [16, 17] for all samples.

$$D = \frac{0.94\lambda}{\beta_{1/2}\cos(\theta)} \qquad (1)$$

Where D is crystallite size, λ is the wavelength of X-ray and $\beta_{1/2}$ is the half-full width of the mean peaks. The X-ray diffraction result were supported by the tolerance factor calculation

$$t = \frac{(r_A + r_o)}{\sqrt{2}\,(\frac{r_B}{2} + \frac{r_{B`}}{2} + r_o)} \qquad (2)$$

Where $r_A, r_o, r_B, r_{B'},$ are the ionic radii of ions of $A_2BB'O_6$ double perovskite [18-20].

2.3. Scanning electronic microscopy

A Jeol JSM 6360 high-resolution scanning electron microscope Stereo-scan LEO 440 used as a tool to investigate the morphology of the sample as well as to determine the homogeneity of the sample, and to obtain the crystals scale crystallization.

2.4. FTIR spectroscopy

At room temperature, the transmittance mode investigated for all samples by a (Satellite FTIR 5000 of the wavelength range of 400 to 4000 cm^{-1}) [21] where the important bands and peaks of perovskite structure can be assigned. A Fourier transform infrared spectroscopy collected by KBr pellet method, the material mixed in KBr of ratio 1:100 for FTIR measurement between 400 and 2000 cm^{-1}.

2.5. Raman spectroscopy

Fourier-transform Raman (FT Raman) spectroscopic analyses were carried out using Bruker: RFS27 (laser 100 mW).

2.6. UV-visible spectroscopy

A UV–visible spectrophotometer (Shimadzu, UV-2550) using $BaSO_4$ as a reference used to calculate the UV– visible diffuse reflectance spectrum at room temperature, the UV.vis Reflectance spectrum converted to absorbance by the Kubella – Munk method to estimate the edge of absorption and band gap of Ba_2NiWO_6 double perovskite powder.

2.7. Photoluminescence

A Perkin Elmer LS55 Fluorescence spectrometer as a tool to investigate Emission and Excitation of Ba_2NiWO_6 double perovskite at room temperature.

3. Results and Discussion

3.1. Structural characterization

3.1.1. Scanning electronic microscopy (SEM) and Energy dispersive X-ray (EDX)

The ESM image and EDX result of Ba_2NiWO_6 series obtained in figure 1. The morphology of the samples is highly homogeneous with no impurities. Some grains have the octahedral shape that appeared clearly in Ba_2NiWO_6 sample, Blum et al. [22] had shown the Sr_2ZnWO_6 octahedral crystal size shape. The lager of the particle size of particles and the particles aggregation in groups observed in the sample, this due to the higher temperature of the preparation. Lan et al. [23] observed the same effect of temperature in the morphology of La_2NiMnO_6 double perovskite oxide. Furthermore, the image reveal the presence of small fine fragments that produced during the preparation grinding. The sample pose a various grain size found in range 0.25- 2 µm.

The EDX analysis taken for sample with SEM image shown in figure 2 that obtained the energy dispersive X-ray spectrum from the element that formed the sample. EDX graph confirm that the elements of the raw material preparation composition and proportion approximating the input quantities of sample with small error, this refer to the homogeneity and crystals purity that shown in table1.

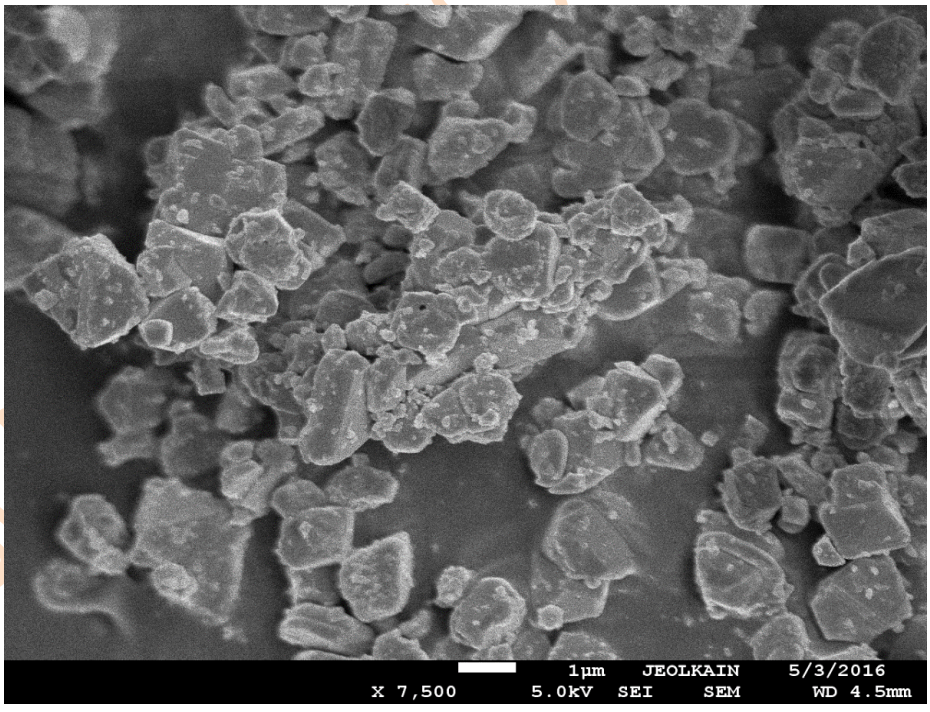

Figure 1. SEM images result of the Ba_2NiWO_6.

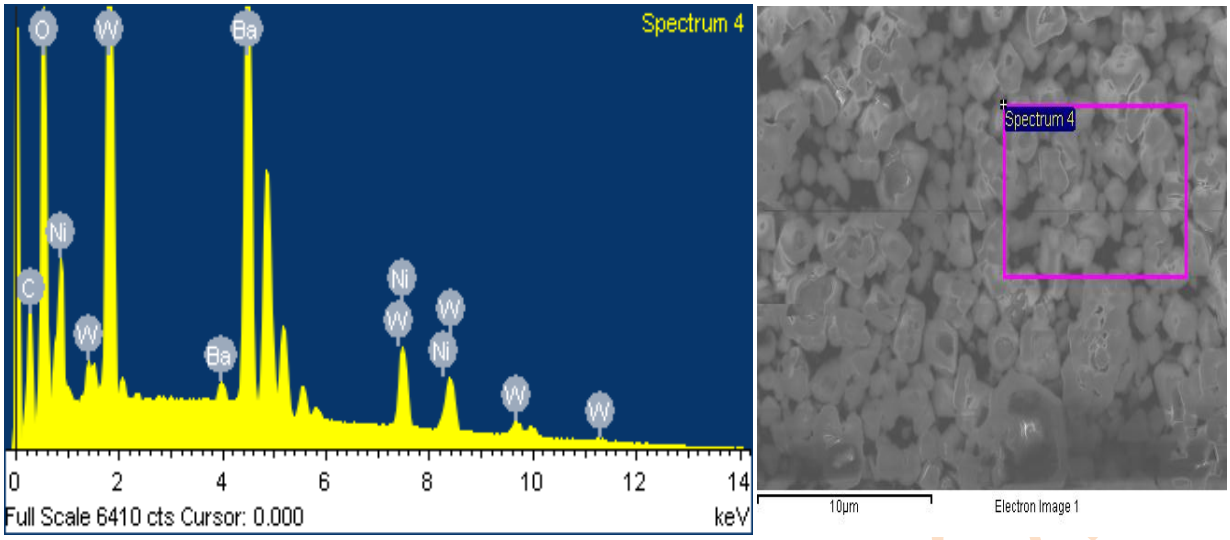

Figure 2. EDX result of the Ba_2NiWO_6.

Table 1. Show the Energy EDX result of Ba_2NiWO_6 double perovskite

Element	Weight%	Atomic%
C K	5.15	22.75
O K	12.91	42.82
Ni K	9.98	9.02
Ba L	47.34	18.30
W M	24.63	7.11
Totals	100.00	

3.1.2. XRD result

The X-ray diffraction data of perovskite oxide compounds are very important to determine the crystalline structure of the sample such as; the Braves crystal [24], atomic position, lattice parameter and space group. Many studies refer the importance of the structure study of materials because they governed the other properties of materials [25]. The XRD of Ba_2NiWO_6 double perovskite oxide that prepared by the solid-state reaction is shown in Figure 3. The $BaWO_4$, Ba_2WO_5 phases were present as a minor peaks at low intensity in the XRD pattern shown in Figure 3 are attributed to impurities in Ba_2NiWO_6 structure around 26.5° and 28° the impurities peaks referred with a plus sign and the star at 2θ around 26.5° and 28° for the $BaWO_4$, Ba_2WO_5 respectively. The XRD data of the sample refined by Rietveld method using fullprof program. The sample obtained in (Fm-3m) cubic crystal structure, Table 2 shows the atoms coordinates of the sample. Figures 4 show the XRD refinement of Ba_2NiWO_6, which structure represent as (Fm-3m) cubic structure with a=b=c= 8.08068Å, α=β=γ 90° lattice parameters. Our result in match with the

Ba_2ZnWO_6 by the Single-crystal X-ray diffraction and Neutron diffraction [27]. Furthermore, $Ba_{2-x}Sr_xMgTeO_6$ ($0 \leq x \leq 1.5$) series found in (Fm-3m) cubic crystal structure [28]. The crystallite size calculated from FWHM at the major peaks at (220) for Ba_2NiWO_6 double perovskite s by Scherer equation found to be 148.7nm for the samples. The tolerance factor found to be 1.020. This is confirmed the (Fm-3m) cubic structure according to the criteria adopted by Correa et al. and Popov et al. [12, 13]. Serrate et al. [29] verified the rule of double perovskite tolerance factor for the (Fm-3m) cubic structure to be between 1.05 - 1.00. Table 3 shows the tolerance factor and the parameter of crystal structure of Ba_2NiWO_6 following Rietveld method refinement

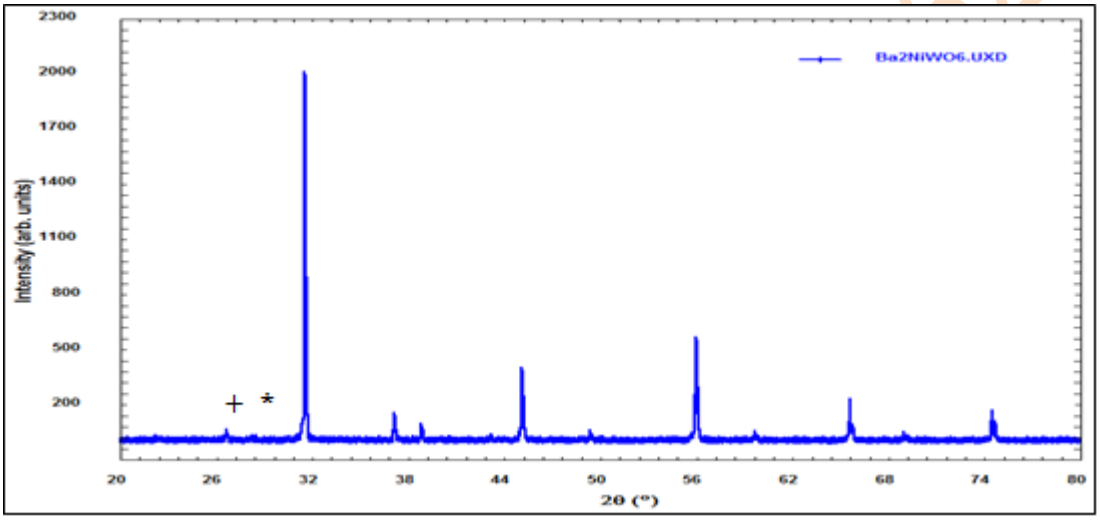

Figure 3. The XRD results of the Ba_2NiWO_6 sample.

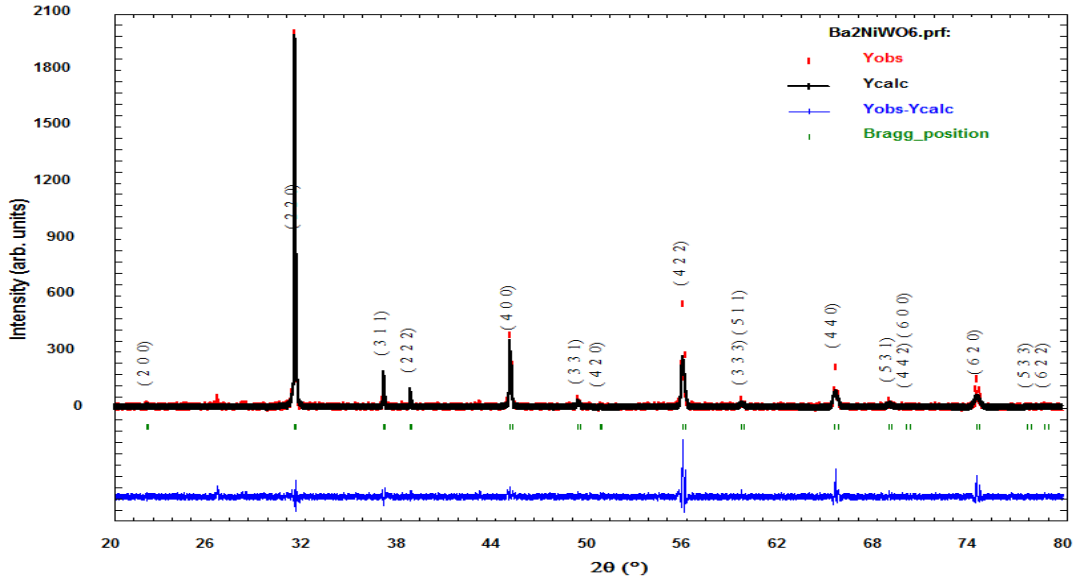

Figure 4. Refined XRD patterns of the Ba_2NiWO_6 sample

Table 2. Atom coordinates of Ba_2NiWO_6 double perovskite following Rietveld refinement of x- ray powder diffraction.

Element	Coordinates	Ba_2NiWO_6 (Fm-3m)
Ba_1^{+2} / Ba_2^{+2}	X	0.25
	Y	0.25
	Z	0.25
Ni^{+2} cation	X	0.5
	Y	0.5
	Z	0.5
W^{+6} cation	X	0
	Y	0
	Z	0
O_1^{-2}/ O_2^{-2} Anions	X	0.23318
	Y	0
	Z	0

Table 3.The tolerance factor and the parameter of crystal structure of Ba_2NiWO_6 following Rietveld method refinement.

Empirical formula	Ba_2NiWO_6
$a(\dot{A})$	8.08068
α/β/γ	90
$V(\dot{A}^3)$	527.648
D(nm)	148.7
T	1.02

3.2. Optical characterization

3.2.1. FTIR spectroscopy

The FTIR spectra identify the crystal structure of the perovskite structure materials that has characteristic absorption bands into 850 - 400 cm^{-1} region [30]. The strong high-energy anti-symmetric stretching mode of the (W–O_6) octahedral was showed at 620 cm^{-1} is due to the higher charge of tungsten cations. The symmetric stretching vibration of WO_6 octahedral appeared as high intensity band at about 825 cm^{-1}. From Figure 5 that shows the transmittance of $BaNiWO_6$ double perovskite versus wave number; the sample confirmed the molecular bonds on the form perovskite oxide form [24].

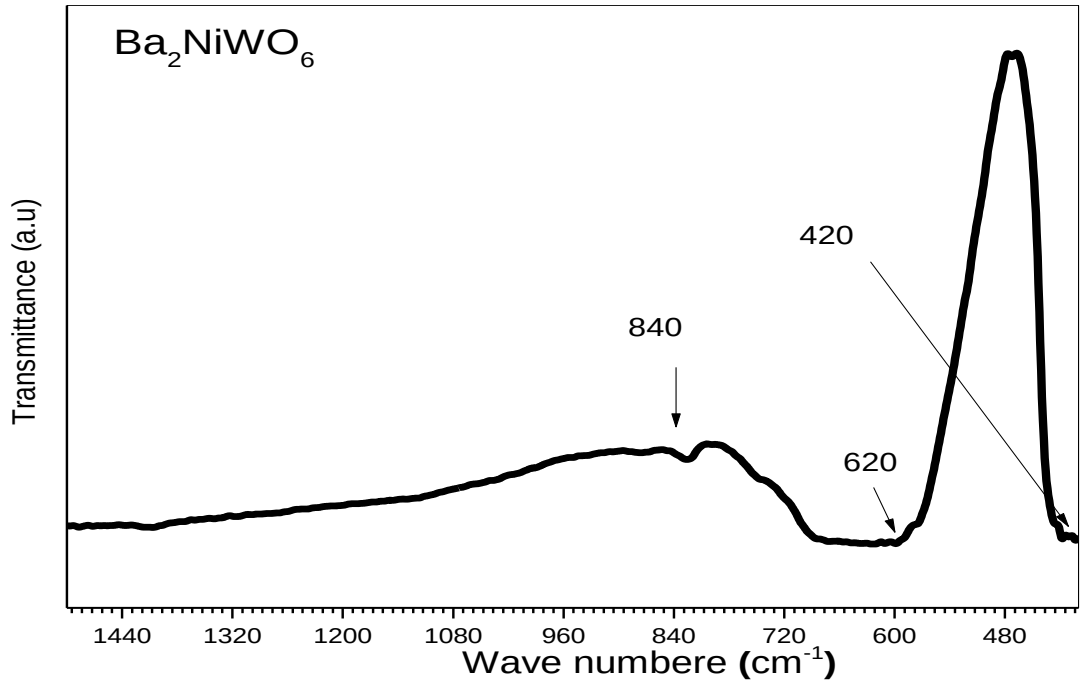

Figure 5. The FTIR spectra of the Ba2NiWO6 double perovskite.

3.2.2 Raman spectroscopy

The Raman spectra of the sample showed in figure.6, the Raman mode classified into two part of lattice vibrations, the W-O-W bending vibration in the 200-500 cm^{-1} region and W-O stretching mode between700-950 cm^{-1}.

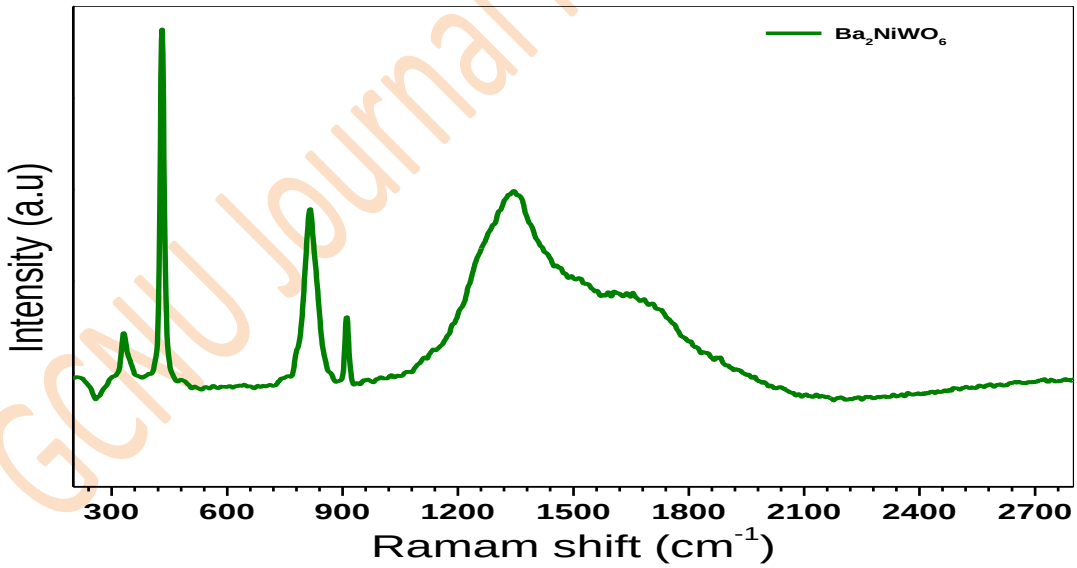

Figure 6: Raman spectra of Ba_2NiWO_6 double perovskite.

3.2.3. UV-VIS diffuse reflectance characterization

Figure 7(a). Show the diffuse reflectance spectrum of the Ba_2NiWO_6 at room temperature in the range of 200-800nm of spectrum. The strong absorption band observed between 300- 450 nm that refer to

the absorption edge in tungsten due to the charge transfer transition of $W^{6+} - O^{2-}$ in the lattice from the highest filled molecular orbital 2p of oxygen to the lowest empty molecular orbital 5d of tungsten. The absorption coefficient calculated for the Ba_2NiWO_6 series from the diffuse reflectance data using the Kubelka-Munk function [31].

$$F(R_\infty) = \frac{\alpha}{s} = \frac{(1-R)^2}{2R} \qquad (3)$$

Where $F(R_\infty)$ is the KM function, α is the absorption coefficient, s is the scattering coefficient and R indicate to the reflection coefficient. The kubelka-munk function (absorbance) shows in relation with wavelength in Figure 7(b). The absorbance can used to observe the absorption edge for the sample that shows in 377 nm for Ba_2NiWO_6. The band gap energy of sample calculated from the absorption edge according to the relationship, $E_g = 12340/\lambda$ (λ is the absorption edge wavelength and the energy gap found to be $E_g = 3.29\, eV$ is band gap as show by [32]). In addition, the band gap energy was calculated for sample by Tauc plot [23] that shown in figure 7(c) according to Eq. (4).

$$[F(R_\infty)h\nu)]^n = A(h\nu - E_g) \qquad (4)$$

Where $h\nu$ is the incident photon energy, A: a proportional constant and E_g is the band gap energy and n takes 2 or 0.5 values for the direct and in direct transition respectively, from Touc plot that found to be $E_g = 3.32\, eV$. Through the study of UV-visible diffuse reflectance and optical energy gap of the sample classified as semiconductor materials [33, 34].

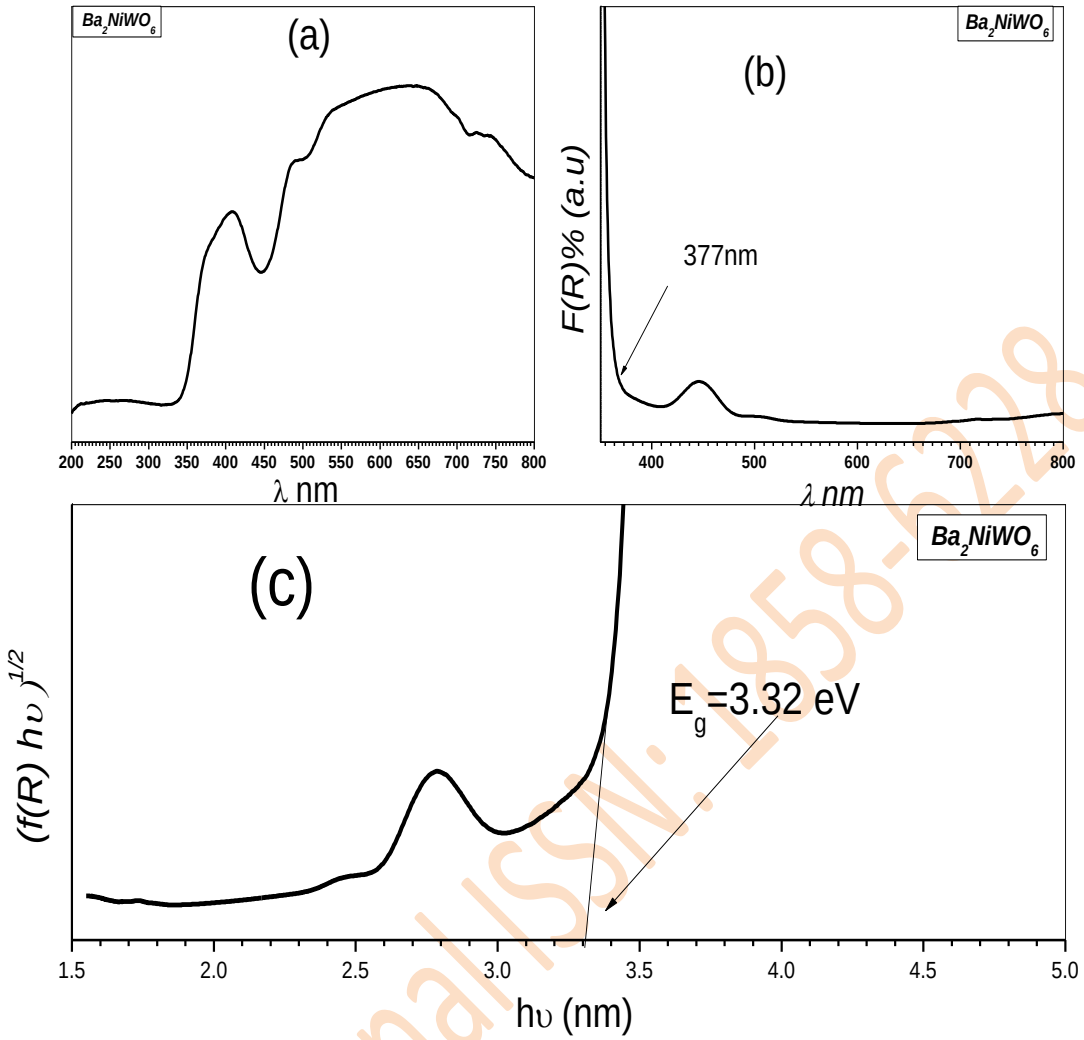

Figure 7 (a)-UV-Vis diffuse reflectance spectra of Ba_2NiWO_6 , (b) - the absorption spectra of Ba_2NiWO_6 as calculated by the Kubelka-Munk function, (c) – dependence of $(h\nu)^{1/2}$ on photon energy $(h\nu)$ for Ba_2NiWO_6.

3.2.4. Fluorescence spectroscopy.

Figure.8a. Shows the Excitation spectra and photoluminescence emission (PLE) spectra of Ba_2NiWO_6 double perovskite oxide. The excitation spectra shown in figure.9b.were collected when $\lambda_{em} = 345nm$ for Ba_2NiWO_6. That consist a broad band between 250 - 350 nm was noticed, this resulting of electronic excitation of O (2p) orbital-W (5d) orbital in octahedral WO_6 [35, 36]. The photoluminescence emission of the sample investigated at $\lambda_{ex} = 290nm$ that spectral emission spread between the 315 to 500 nm. Bugaris et al. [34] found a complimentary result which the emission peak of Ba_2ZnWO_6 has its maximum at 539 nm when $\lambda_{ex} = 380nm$. The PLE of Ba_2NiWO_6 have peaks at 343, 342, 341 nm with FWHM 60 nm.

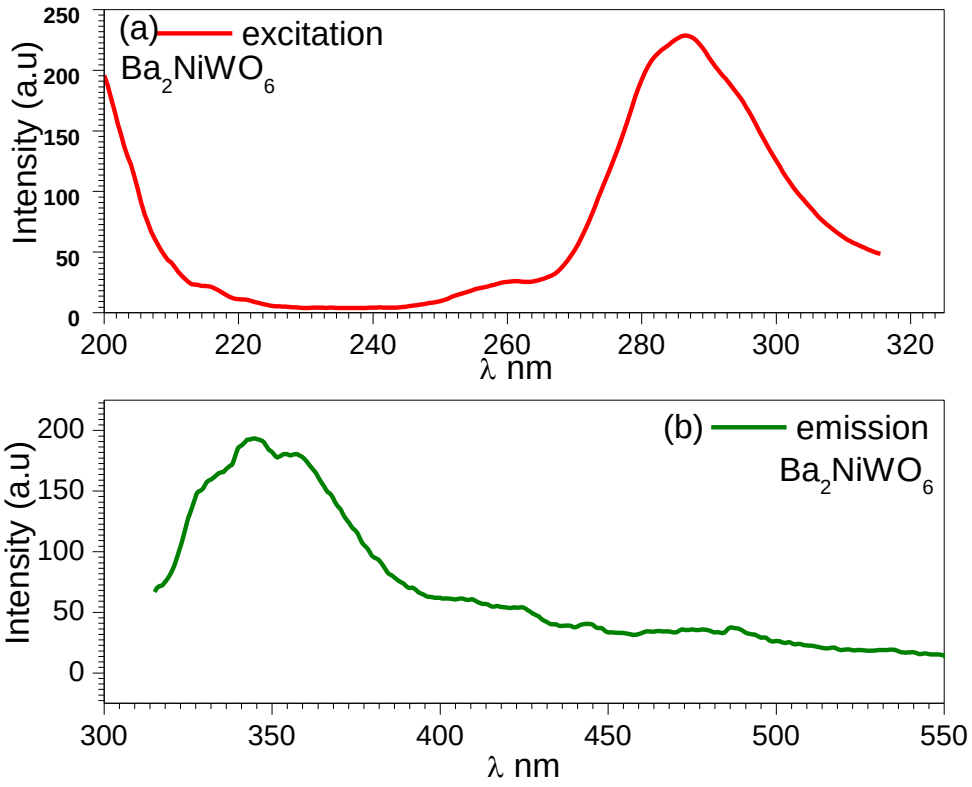

Figure 9 (a) PLE spectra (λ_{em} =380 nm); (b) PL spectra (λ_{ex} =290 nm) of Ba_2NiWO_6 sample.

3.2.5. Impedance spectroscopy.

In order to understand the dynamics of the mobile ions (dielectric relaxation) in Ba_2NiWO_6 double perovskite , we have plotted the complex plane impedance plots Z^*in figure 9.(a) and we have plotted the logarithmic of frequency dependence of the real and imaginary parts of the complex electrical impedance of Ba_2NiWO_6 in figure 9.(b), (c). The Z^* plots not only provide information about the electrical properties of Ba_2NiWO_6, but also an idea of the relaxation mechanism[37]. The Z^* plot of all sample shows the semicircular arc with it center lying below the real axis of the Z^*.

The high frequency semicircular arc in Ba_2NiWO_6 cases can be attributed to the contribution from Bulk material arising due to parallel combination of the grain resistance R_g and grain capacitance C_g. the equivalent electrical circuit from the same is shown in figure.10 where the Z^* can calculated by the below equation[38].

$$Z^* = Z' - Z'' = \frac{1}{R_g^{-1} + jwC_g} \quad , \qquad Z' = \frac{R_g}{1+(\omega R_g C_g)^2} \quad , \qquad Z'' = R_g\left[\frac{\omega R_g C_g}{1+(\omega R_g C_g)^2}\right]$$

No residual semicircular at low frequencies attributed to the contact or electrode effects has been noticed in Ba_2NiWO_6 cases, probably due to the fact that samples were well polished and taken good sintering before conducting the sample in the EIS Machin[39].

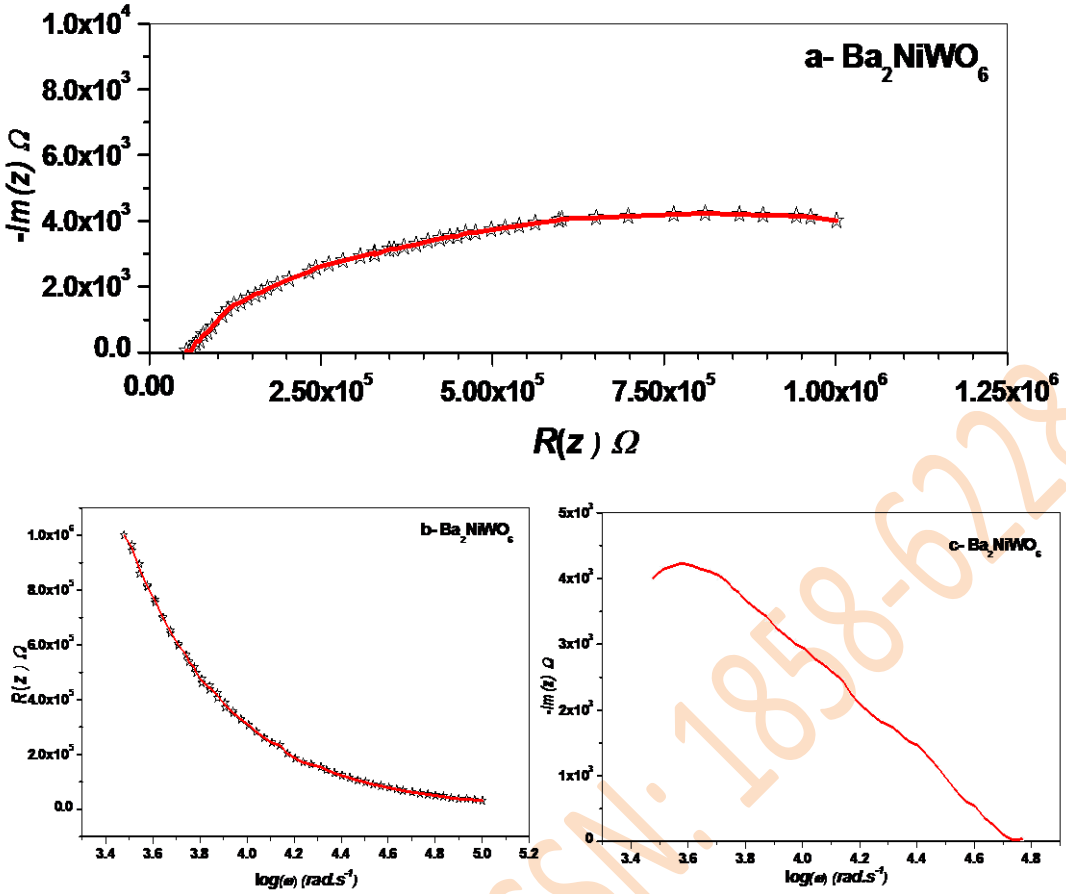

Figure 9(a) -The complex Cole-Cole plot (b) - The Bode real dielectric (C) - The Bode imaginary dielectric impedance data measured of the Ba_2NiWO_6.

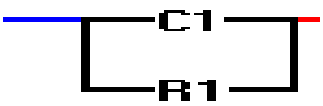

Figure.10 equivalent circuit of Ba_2NiWO_6.

Figure 9(b) shows the variation of the real part of impedance ($Z^{'}$) of the sintered pellet of $Ba_2Zn_{1-x}Ni_xWO_6$ series measured in the logarithmic frequency (frequency range 10^3 Hz – 10^6 Hz). The real part of impedance relaxation shown get significant variation with frequency that falls from high values in low frequency to the nearer zero ohm in high frequency around 10^6Hz. Also the variation of imaginary part of impedance ($Z^{''}$) of Ba_2NiWO_6 on the logarithmic frequency (frequency range 10^3 Hz – 10^6 Hz). The study revealed that the imaginary part of impedance does not show the significant variation with frequency and it falls zero Ω. whereas, the imaginary part relaxation shown variation

with frequency that falls from high values in low frequency to the zero ohm in high frequency around 10^6Hz.

4. Conclusion

The double perovskite oxide with formula Ba_2NiWO_6 prepared by conventional solid-state reaction method. The sample kept the cubic crystal structure. The size of grins of series obtained in microstructure size. The EDX result confirm the ratio of the element comprise internal of 2:1: for Ba, Ni, and W of the Ba_2NiWO_6. A strong absorption at 620 cm^{-1} was show by FTIR due to the anti-symmetric stretching mode of W - O_6 octahedral. The band gap of 3.29 eV from the absorption edge is closer to the value of 3.23 eV by Tauce plot .The absorption and optical band gap energy classified the series as semiconductor materials. The luminescence and EIS spectroscopy observed for the Ba_2NiWO_6.

References:

1. Lufaso MW. Perovskite synthesis and analysis using structure prediction diagnostic software: The Ohio State University; 2002.

2. Galasso FS. Structure, Properties and Preparation of Perovskite-Type Compounds: International Series of Monographs in Solid State Physics: Elsevier; 2013.

3. Knapp MC. INVESTIGATIONS INTO THE STRUCTURE AND PROPERTIES OF ORDERED PEROVSKITES, LAYERED PEROVSKITES, AND DEFECT PYROCHLORES: The Ohio State University; 2006.

4. Yang S, Yan N, Chenl S, Zhang Y. Structural and optical properties of $BiFeO_3$ system multiferroic films prepared by sol-gel method. Ceramics International. 2015.

5. Bharti C, Das MK, Sen A, Chanda S, Sinha T. Rietveld refinement and dielectric relaxation of a new rare earth based double perovskite oxide: $BaPrCoNbO_6$. Journal of Solid State Chemistry. 2014;210(1):219-23.

6. Landínez Téllez DA, Martínez Buitrago D, Cardona C R, Barrera EW, Roa-Rojas J. Journal of Molecular Structure. 2014;1067(0):205-9.

7. Min L, Hong-ming Y, Wei X, Mei H, Lin-ran Y, Ming Y, et al. Hydrothermal Synthesis and Dielectric Characterization of a Double Perovskite Ba_2FeSbO_6. CHEMICAL RESEARCH IN CHINESE UNIVERSITES. 2012;28(5):788-91.

8. Feraru S, Samoila P, Borhan A, Ignat M, Iordan A, Palamaru M. Synthesis, characterization double perovskite Ca_2 $MSbO_6$ (M= Dy, Fe, Cr, Al) materials via sol–gel auto-combustion and their catalytic properties. Materials Characterization. 2013;84:112-9.

9. Elbadawi AA, Yassin OA, Gismelseed AA. Effect of the internal pressure and the anti-site disorder on the structure and magnetic properties of $ALaFeTiO_6$ (A=Ca, Sr, Ba) double perovskite oxides. Journal of Magnetism and Magnetic Materials. 2013;326(0):1-6.

10. Kim H-S, Lee C-R, Im J-H, Lee K-B, Moehl T, Marchioro A, et al. Lead Iodide Perovskite Sensitized All-Solid-State Submicron Thin Film Mesoscopic Solar Cell with Efficiency Exceeding 9%. Scientific Reports. 2012;2:591.

11. Peschel S, Ziegler B, Schwarten M, Babel D. Kristallstrukturbestimmungen an $Cs_2NaCr(CN)_6$ und weiteren Verbindungen $A_2BM(CN)_6$ (A=Rb, Cs; B=Na, K, Rb, NH_4; M=Cr, Mn, Fe, Co): Oktaederkippung und Toleranzfaktor von Cyanokryolithen. Zeitschrift für anorganische und allgemeine Chemie. 2000;626(7):1561-6.

12. Landínez Téllez DA, Martínez Buitrago D, Cardona C R, Barrera EW, Roa-Rojas J. Crystalline structure, magnetic response and electronic properties of RE_2MgTiO_6 (RE=Dy, Gd) double perovskites. Journal of Molecular Structure. 2014;1067(0):205-9.

13. Shaikh MW, Varshney D. Structural properties and electrical resistivity behaviour of $La_{1-x}K_xMnO_3$ (x = 0.1, 0.125 and 0.15) manganites. Materials Chemistry and Physics. 2012;134(2–3):886-98.

14. Sundarayya Y, Mandal P, Sundaresan A, Rao CNR. Mössbauer spectroscopic study of spin reorientation in Mn-substituted yttrium orthoferrite. Journal of Physics: Condensed Matter. 2011;23(43):436001.

15. Suryanarayana C, Norton MG. X-Rays and Diffraction. X-Ray Diffraction: Springer; 1998. p. 3-19.

16. Tuza PV, Souza MM. Steam Reforming of Methane Over Catalyst Derived from Ordered Double Perovskite: Effect of Crystalline Phase Transformation. Catalysis Letters. 2016;146(1):47-53.

17. Alsabah YA, Elbadawi AA, Mustafa EM, Siddig MA. The Effect of Replacement of Zn^{2+} Cation with Ni^{2+} Cation on the Structural Properties of $Ba_2Zn_{1-x}Ni_xWO_6$ Double Perovskite Oxides (X= 0, 0.25, 0.50, 0.75, 1). Journal of Materials Science and Chemical Engineering. 2016;4(02):61.

18. Nilsen GJ, Thompson CM, Ehlers G, Marjerrison CA, Greedan JE. Diffuse magnetic neutron scattering in the highly frustrated double perovskite Ba_2YRuO_6. Physical Review B. 2015;91(5):054415.

19. Corrêa H, Cavalcante I, Souza D, Santos E, Orlando MD, Belich H, et al. Synthesis and structural characterization of the Ca_2MnReO_6 double perovskite. Cerâmica. 2010;56(338):193-200.

20. Gandhi A, Keshri S. Microwave dielectric properties of double perovskite ceramics. Ceramics International. 2015;41(3, Part A):3693-700.

21. Kavitha VT, Jose R, Ramakrishna S, Wariar PRS, Koshy J. Combustion synthesis and characterization of Ba_2NdSbO_6 nanocrystals. Bull Mater Sci. 2011;34(4):661-5.

22. Blum CGF, Holcombe A, Gellesch M, Sturza MI, Rodan S, Morrow R, et al. Flux growth and characterization of Sr2NiWO6 single crystals. Journal of Crystal Growth. 2015;421:39-44.

23. Lan C, Zhao S, Xu T, Ma J, Hayase S, Ma T. Investigation on structures, band gaps, and electronic structures of lead free La_2NiMnO_6 double perovskite materials for potential application of solar cell. Journal of Alloys and Compounds. 2016;655:208-14.

24. Yang W, Lee W. Introduction to Material Structures. Mesoplasticity and its Applications: Springer; 1993. p. 64-110.

25. Elbadawi AA, Yassin O, Siddig MA. Effect of the Cation Size Disorder at the A-Site on the Structural Properties of $SrAFeTiO_6$ Double Perovskites (A= La, Pr or Nd). Journal of Materials Science and Chemical Engineering. 2015;3(05):21.

26. Manoun B, Ezzahi A, Benmokhtar S, Ider A, Lazor P, Bih L, et al. X-ray diffraction and Raman spectroscopy studies of temperature and composition induced phase transitions in $Ba_{2-x}Sr_xZnWO_6$ ($0 \leq x \leq 2$) double perovskite oxides. Journal of Alloys and Compounds. 2012;533:43-52.

27. Bugaris DE, Hodges JP, Huq A, zur Loye H-C. Crystal growth, structures, and optical properties of the cubic double perovskites Ba_2MgWO_6 and Ba_2ZnWO_6. Journal of Solid State Chemistry. 2011;184(8):2293-8.

28. Tamraoui Y, Manoun B, Mirinioui F, Haloui R, Lazor P. X-ray diffraction and Raman spectroscopy studies of temperature and composition induced phase transitions in $Ba_{2-x}Sr_xMgTeO_6$ ($0 \leqslant x \leqslant 2$). Journal of Alloys and Compounds. 2014;603:86-94.

29. Serrate D, Teresa JMD, Ibarra MR. Double perovskites with ferromagnetism above room temperature. Journal of Physics: Condensed Matter. 2007;19(2):023201.

30. Mostafa MF, Ata-Allah SS, Youssef AAA, Refai HS. Electric and AC magnetic investigation of the manganites $La_{0.7}Ca_{0.3}Mn_{0.96}In_{0.04x}Al_{(1-x)0.04}O_3$; ($0.0 \leqslant x \leqslant 1.0$). Journal of Magnetism and Magnetic Materials. 2008;320(3–4):344-53.

31. Dutta A, Mukhopadhyay P, Sinha T, Shannigrahi S, Himanshu A, Sen P, et al. Sr 2 SmNbO 6 perovskite: Synthesis, characterization and density functional theory calculations. Materials Chemistry and Physics. 2016.

32. Chen F, Niu C, Yang Q, Li X, Zeng G. Facile synthesis of visible-light-active BiOI modified Bi_2MoO_6 photocatalysts with highly enhanced photocatalytic activity. Ceramics International. 2016;42(2, Part A):2515-25.

33. Kittel C, Holcomb DF. Introduction to solid state physics. American Journal of Physics. 1967;35(6):547-8.

34. Bugaris DE, Hodges JP, Huq A, Zur Loye H-C. Crystal growth, structures, and optical properties of the cubic double perovskites Ba_2MgWO_6 and Ba_2ZnWO_6. Journal of Solid State Chemistry. 2011;184(8):2293-8.

35. Xu D, Yang Z, Sun J, Gao X, Du J. Synthesis and luminescence properties of double-perovskite white emitting phosphor $Ca_3WO_6:Dy^{3+}$. Journal of Materials Science: Materials in Electronics. 2016:1-8.

36. Xiao N, Shen J, Xiao T, Wu B, Luo X, Li L, et al. $Sr_2CaW_xMo_{1-x}O_6:Eu^{3+}$, Li^+: An emission tunable phosphor through site symmetry and excitation wavelength. Materials Research Bulletin. 2015;70:684-90.

37. Bharti C, Sen A, Chanda S, Sinha TP. Structural, vibrational and electrical properties of ordered double perovskite oxide $BaLaMnSbO_6$. Journal of Alloys and Compounds. 2014;590:125-30.

38. Mahato DK, Dutta A, Sinha T. Synthesis and electric characterization of rare earth double perovskite Ho_2CdZrO_6 ceramics. Journal of electroceramics. 2012;29(2):99-105.

39. Bharti C, Sinha TP. Synthesis, crystal structure, dielectric and optical properties of a new rare earth double perovskite: Ca_2CeNbO_6. Physica B: Condensed Matter. 2012;407(1):84-9.